Supplement to

Bias characterization of OMI HCHO columns based on FTIR and aircraft measurements and impact on top-down emission estimates

Jean-François Müller[1], Trissevgeni Stavrakou[1], Glenn-Michael Oomen[1], Beata Opacka[1], Isabelle De Smedt[1], Alex Guenther[2], Corinne Vigouroux[1], Bavo Langerock[1], Carlos Augusto Bauer Aquino[3], Thomas Blumenstock[4], Michel Grutter[5], James W. Hannigan[6], Rigel Kivi[7], Erik Lutsch[8], Emmanuel Mahieu[9], Maria Makarova[10], Jean-Marc Metzger[11], Isamu Morino[12], Isao Murata[13], Tomoo Nagahama[14], Justus Notholt[15], Ivan Ortega[6], Mathias Palm[15], Amelie Röhling[4], Wolfgang Stremme[5], Kimberly Strong[8], Ralf Sussmann[16], Yao Té[17], Alan Fried[18]

[1] Royal Belgian Institute for Space Aeronomy, Avenue Circulaire 3, 1180, Brussels, Belgium [2] University of California Irvine, Irvine, CA, USA [3] Instituto Federal de Educaçao, Ciência e Tecnologia de Rondônia (IFRO), Porto Velho, Brazil [4] Karlsruhe Institute of Technology (KIT), Institute for Meteorology and Climate Research (IMK-ASF), Karlsruhe, Germany [5] Instituto de Ciencias de la Atmósfera y Cambio Climático, Universidad Nacional Autónoma de México (UNAM), Mexico City, México [6] Atmospheric Chemistry, Observations & Modeling, National Center for Atmospheric Research (NCAR), Boulder, CO, USA [7] Finnish Meteorological Institute (FMI), Sodankylä, Finland [8] Department of Physics, University of Toronto, Toronto, Canada [9] Institut d'Astrophysique et de Géophysique, Université de Liège, Liège, Belgium [10] Saint Petersburg State University, Atmospheric Physics Department, St. Petersburg, Russia [11] Observatoire des Sciences de l'Univers Réunion (OSU-R), UMS 3365, Université de la Réunion, Saint-Denis, France [12] National Institute for Environmental Studies (NIES), Tsukuba, Ibaraki 305-8506, Japan [13] Graduate School of Environment Studies, Tohoku University, Sendai 980-8578, Japan [14] Institute for Space-Earth Environmental Research (ISEE), Nagoya University, Nagoya, Japan [15] Institute of Environmental Physics, University of Bremen, Bremen, Germany [16] Karlsruhe Institute of Technology, IMK-IFU, Garmisch-Partenkirchen, Germany [17] LERMA-IPSL, Sorbonne Université, CNRS, Observatoire de Paris, PSL Université, 75005 Paris, France [18] Institute of Arctic and Alpine Research, University of Colorado, Boulder, CO, USA

Atmospheric Chemistry and Physics, 2023

This supplement contains 11 figures and 5 tables which support the main manuscript.

Table S1. FTIR stations contributing in this work: longitude, latitude, altitude above sea level, retrieval code and team.

Station		Latitude North	Longitude East	Altitude (km)	Code	Team
Eureka	EUR	80.05	-86.42	0.61	SFIT4	U. Toronto
Ny-Ålesund	NYA	78.92	11.92	0.02	SFIT4	U. Bremen
Thule	THU	76.52	-68.77	0.22	SFIT4	NCAR
Kiruna	KIR	67.84	20.40	0.42	PROFFIT	KIT-ASF; IRF Kiruna
Sodankylä	SOD	67.37	26.63	0.19	SFIT4	FMI; BIRA
St. Petersburg	SPE	59.88	29.83	0.02	SFIT4	SPbU
Bremen	BRE	53.10	8.85	0.03	SFIT4	U. Bremen
Paris	PAR	48.97	2.37	0.06	PROFFIT	Sorbonne U.
Garmisch	GAR	47.48	11.06	0.74	PROFFIT	KIT-IFU
Zugspitze	ZUG	47.42	10.98	2.96	PROFFIT	KIT-IFU
Junfraujoch	JFJ	46.55	7.98	3.58	SFIT4	U. Liège
Toronto	TOR	43.60	-79.40	0.17	SFIT4	U. Toronto
Rikubetsu	RIK	43.46	143.77	0.38	SFIT4	Nagoya U.; NIES
Boulder	BOU	40.04	-105.24	1.61	SFIT4	NCAR
Tsukuba	TSU	36.05	140.12	0.03	SFIT4	NIES; Tohoku U.
Hefei	HEF	31.91	117.17	0.03	SFIT4	HFIPS; CAS
Izaña	IZA	28.30	-16.48	2.37	PROFFIT	AEMET; KIT-ASF
Mauna Loa	MLO	19.54	-155.57	3.40	SFIT4	NCAR
Mexico City (UNAM)	MEX	19.33	-99.18	2.26	PROFFIT	UNAM
Altzomoni	ALT	19.12	-98.66	3.98	PROFFIT	UNAM
Paramaribo	PAM	5.81	-55.21	0.03	SFIT4	U. Bremen
Porto Velho	PVO	-8.77	-63.87	0.09	SFIT4	BIRA
La Réunion – St.Denis	SDE	-20.90	55.48	0.08	SFIT4	BIRA
La Réunion – Maïdo	MAI	-21.08	55.38	2.16	SFIT4	BIRA
Wollongong	WOL	-34.41	150.88	0.03	SFIT4	U. Wollongong
Lauder	LAU	-45.04	169.68	0.37	SFIT4	NIWA

Table S2. A priori and optimized annual NMVOC emissions over the model domain (10-54°N, 65-130°W) in the aircraft-based inversion (TgVOC yr^{-1}).

	A priori	Optimized
Biomass burning		
2012	2.5	3.4
2013	5.1	6.1
Anthropogenic		
2012	19.7	98.3
2013	19.7	88.7
Biogenic		
2012	37.9	36.4
2013	32.8	31.6
Total		
2012-2013 average	118	264

Table S3. Impact of bias correction on top-down NMVOC emission totals (Tg year^{-1}) over the same large regions as in Table 3 in the main manuscript. The means are taken over 2011-2017 for optimizations using either uncorrected (OPT1) or bias-corrected OMI HCHO columns (OPT2). The total land surface area of the regions is also given.

	North America	South America	Europe	NH Africa	SH Africa	North Asia	South Asia	Oceania	**Global**
Surface area (10^6 km^2)	22.1	18.0	9.6	25.6	25.6	23.7	14.9	8.0	**147**
Biomass burning NMVOC emissions									
GFED4s 2011–2017	6.6	12.1	1.2	15.7	25.1	7.3	14.3	4.2	**87**
OPT1 (no bias correction)	6.1	9.8	1.7	10.9	23.8	9.4	10.7	4.0	**77**
OPT2 (bias-corrected)	6.1	10.8	1.6	12.2	29.7	8.9	12.5	4.2	**87**
Isoprene emissions									
MEGAN-MOHYCAN 2011–2017	35.2	148.8	6.7	85.6	44.6	9.5	39.1	60.9	**430**
OPT1 (no bias correction)	33.5	107.6	9.0	60.7	59.4	14.6	38.8	34.6	**362**
OPT2 (bias-corrected)	45.3	125.9	12.1	77.3	75.1	17.1	55.8	37.0	**451**
Anthropogenic NMVOC emissions									
EDGAR 2011–2017	20.3	12.8	16.7	41.4	12.3	11.9	54.6	1.1	**179**
OPT1 (no bias correction)	36.0	12.1	23.4	43.6	13.5	16.0	56.7	1.1	**215**
OPT2 (bias-corrected)	20.6	11.6	18.0	36.6	13.3	15.3	62.0	1.1	**192**
Total NMVOC emissions									
A priori 2011–2017	62	174	25	143	82	29	108	66	**701**
OPT1 (no bias correction)	76	129	34	115	97	40	106	40	**654**
OPT2 (bias-corrected)	72	148	32	126	118	41	130	42	**730**

Table S4. Statistics of the comparison between HCHO mixing ratios measurements from aircraft campaigns and the model simulations using a priori emissions (APRI), optimized emissions constrained by OMI without bias-correction (OPT1) or with bias-correction (OPT2). OPT3 is as OPT2, but with doubled errors on the emission parameters (only for 2013 campaigns). n is the number of measurements. The bias (%) is calculated as 100$\times$ (<$C_m - C_o$>)/<C_o>, where C_m and C_o denote the simulated and observed mixing ratios, respectively, and <..> denotes the average over all data from each campaign. The root-mean square deviation (RMSD) is calculated as (< $(C_m - C_o)^2$ >)$^{1/2}$. Only data below 4 km altitude are considered. See Table 1 and Fig. 1 in the main manuscript for additional details on the campaigns.

	n	C_o (ppbv)	Bias APRI %	Bias OPT1 %	Bias OPT2 %	Bias OPT3 %	RMSD APRI ppbv	RMSD OPT1 ppbv	RMSD OPT2 ppbv	RMSD OPT3 ppbv
DC3 (DC8)	1699	1.70	-38	-34	-21	-15	0.66	0.62	0.39	0.30
DC3 (GV)	949	1.55	-29	-23	-2	+4	0.52	0.45	0.34	0.31
SEAC^{4}RS	3385	2.39	+3	-16	+15	+12	0.20	0.48	0.43	0.35
MILAGRO (DC8)	547	1.86	-29	-25	-16		0.67	0.60	0.44	
ARCTAS-CARB	882	2.73	-50	-29	-10		1.53	0.96	0.49	
ARCTAS-B	777	2.41	+11	+6	+9		0.81	0.60	0.61	
DISCOVER-AQ Maryland	3403	2.12	-18	-15	+8		0.64	0.58	0.22	
SENEX	3821	3.70	-30	-38	-7	-10	1.18	1.51	0.38	0.49
DISCOVER-AQ California	3611	1.15	-55	-41	-53	-53	0.80	0.63	0.77	0.78
DISCOVER-AQ Colorado	2379	1.92	-52	-44	-43		1.08	0.94	0.92	
KORUS-AQ	499	1.67	-35	-33	-22		0.69	0.65	0.44	
All campaigns	21952	2.22	-26.6	-28.2	-9.0		0.85	0.86	0.55	

Table S5. Statistics of the comparison between FTIR columns (2011–2017) and model simulations using a priori emissions (APRI), optimized emissions constrained by OMI without bias-correction (OPT1) or with bias-correction (OPT2). n is the number of measurements. The bias (%) is calculated as 100× (<$C_m - C_o$>)/<C_o>, where C_m and C_o denote the simulated and observed columns, respectively, and <..> denotes the average over all data from each station. The root-mean square deviation (RMSD) is calculated as (< $(C_m - C_o)^2$ >)$^{1/2}$.

	n	C_o 10^{15} molec.cm^{-2}	Bias APRI %	Bias OPT1 %	Bias OPT2 %	RMSD APRI ppbv	RMSD OPT1 ppbv	RMSD OPT2 ppbv
Kiruna	624	1.8	+16	+25	+20	0.43	0.57	0.51
Sodankyla	2258	2.3	+6	+15	+11	0.42	0.51	0.43
St.Petersburg	2009	5.9	-18	-10	-13	1.42	1.14	1.11
Bremen	311	5.6	-14	+9	-8	1.79	1.97	1.50
Paris	5068	7.5	-24	-16	-19	2.32	1.86	1.94
Garmisch	2600	5.7	-8	+3	+4	1.25	0.96	0.61
Toronto	1267	9.3	-30	-26	-25	2.59	2.08	2.09
Boulder	409	4.9	-39	-33	-33	3.12	2.67	2.58
Mexico City	3754	25.6	-67	-68	-64	16.79	16.84	15.90
Paramaribo	140	6.2	+21	+6	+4	1.70	1.10	1.03
Porto Velho	433	18.6	+20	-20	-2	5.36	3.89	2.35

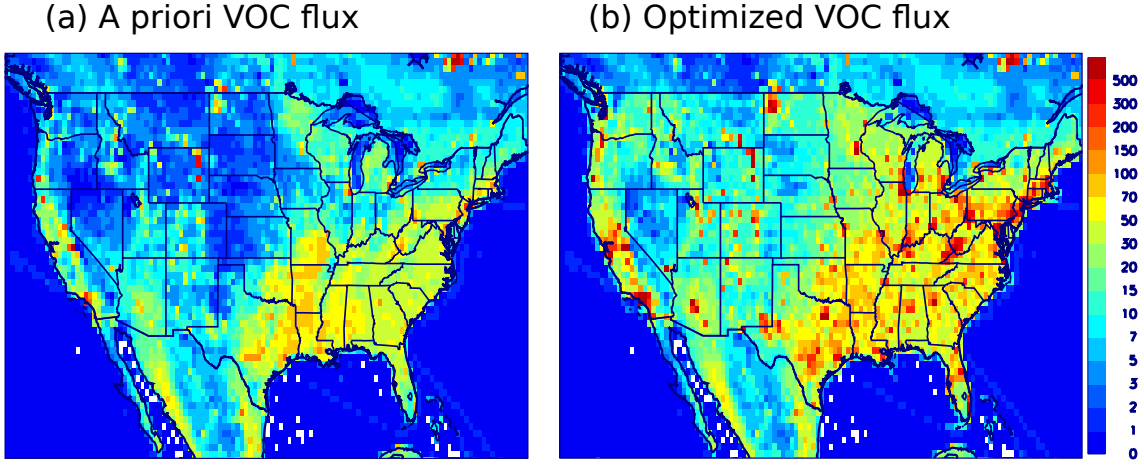

Figure S1. VOC flux distribution (10^{10} molec. cm^{-2} s^{-1}) according to the (a) a priori inventories and (b) the aircraft-based emission inversion. The sum of all three categories (anthropogenic, biomass burning, biogenic) is shown for June-Aug. 2013.

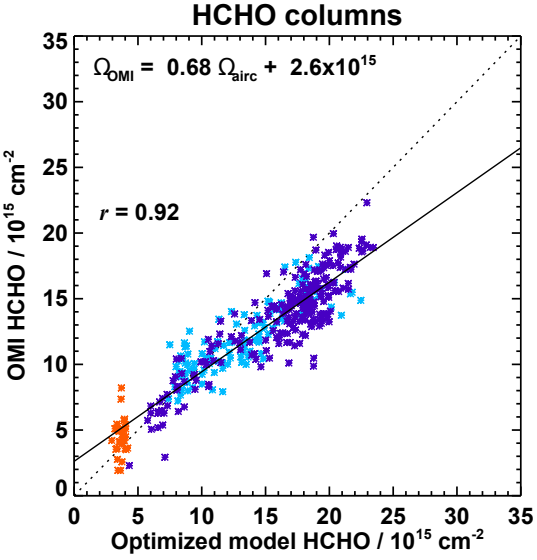

Figure S2. As in Fig. 5b, for the standard cloud-corrected QA4ECV HCHO product. The correlation coefficient, slope and intercept of a linear regression using the Theil-Sen estimator are given. The regression is shown as black solid line.

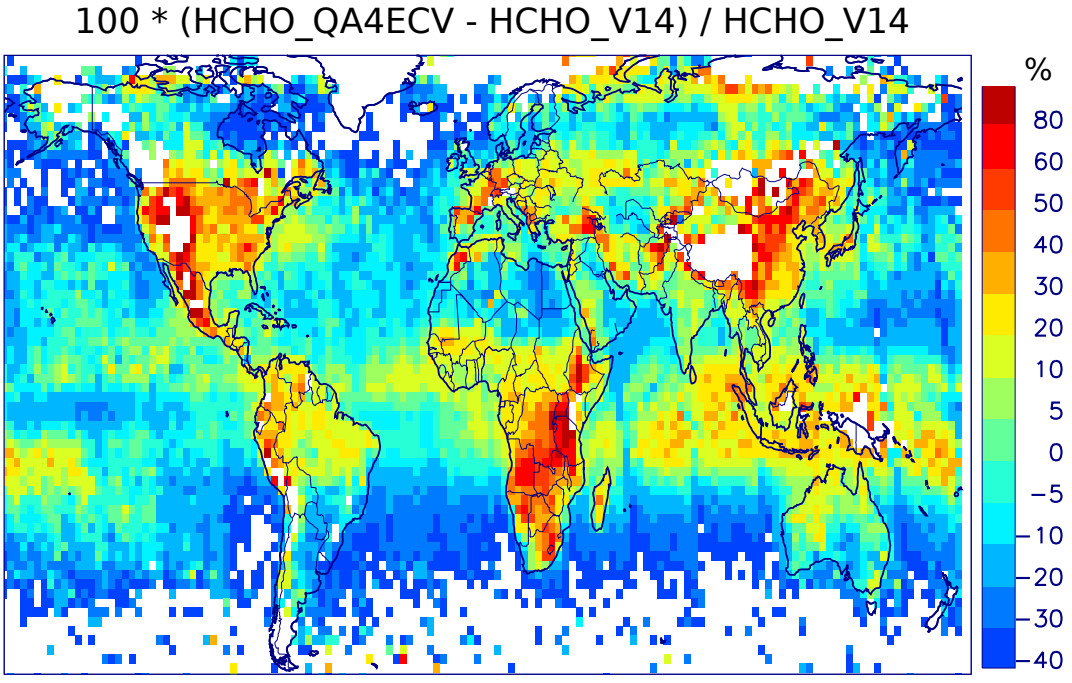

Figure S3. Percentage difference between the yearly-averaged HCHO columns from QA4ECV (with clear-sky air mass factors) and the HCHO columns the from BIRA V14 product (De Smedt et al., 2015). The same cloud filter is applied in both case (cloud fraction < 0.4).

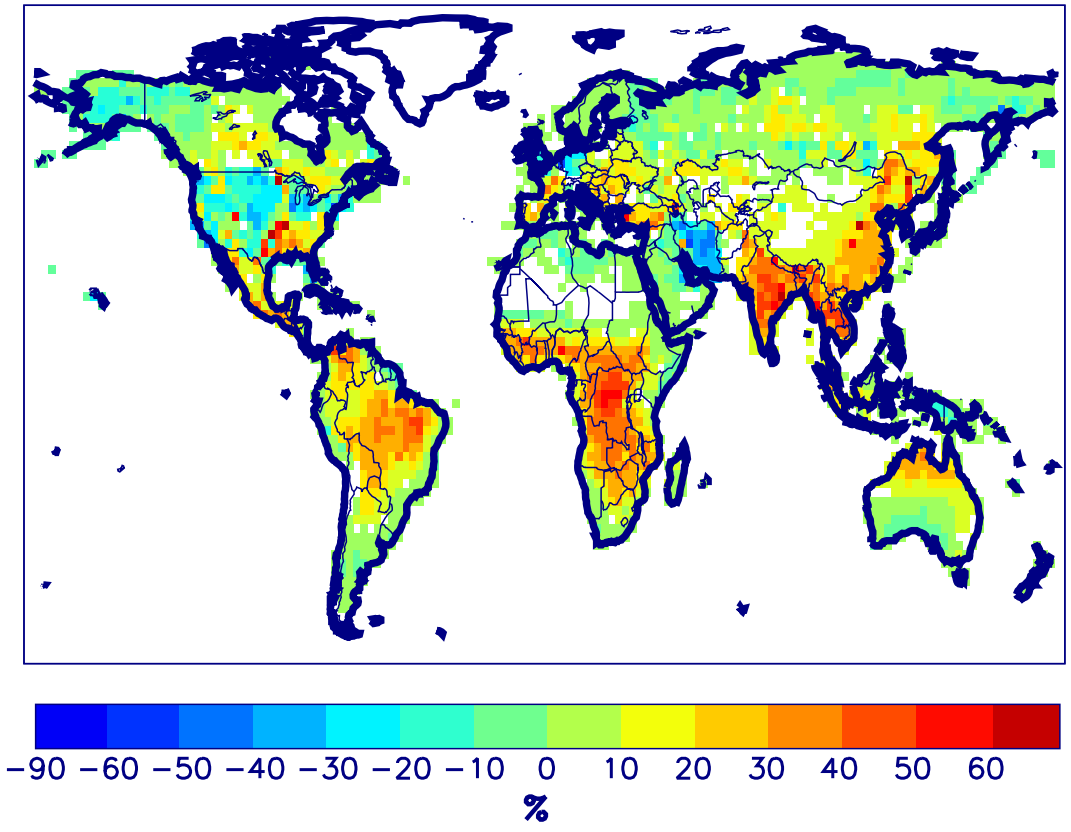

Figure S4. Percentage change in total top-down VOC flux (2011–2017 average) due to the bias correction of OMI data, i.e. between runs OPT1 and OPT2.

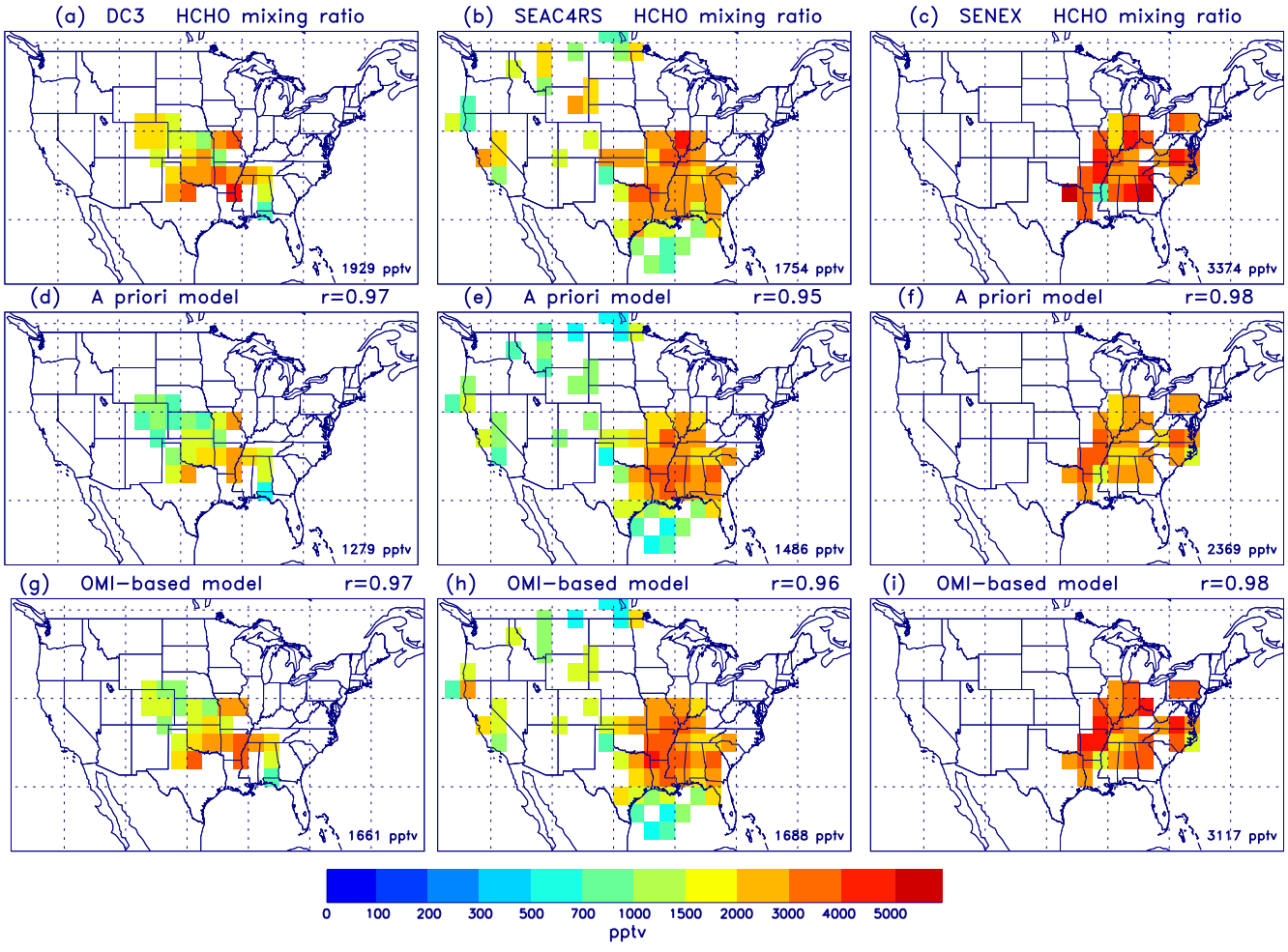

Figure S5. Measured HCHO mixing ratio below 4 km altitude (pptv) from the campaigns (a) DC3, (b) SEAC^{4}RS, and (c) SENEX, and corresponding model distributions using a priori emissions (d, e, f) and with optimized emissions based on bias-corrected OMI (OPT2) (g, h, i). The data were regridded to the model resolution. The average measured or modelled mixing ratio is given inset for each campaign.

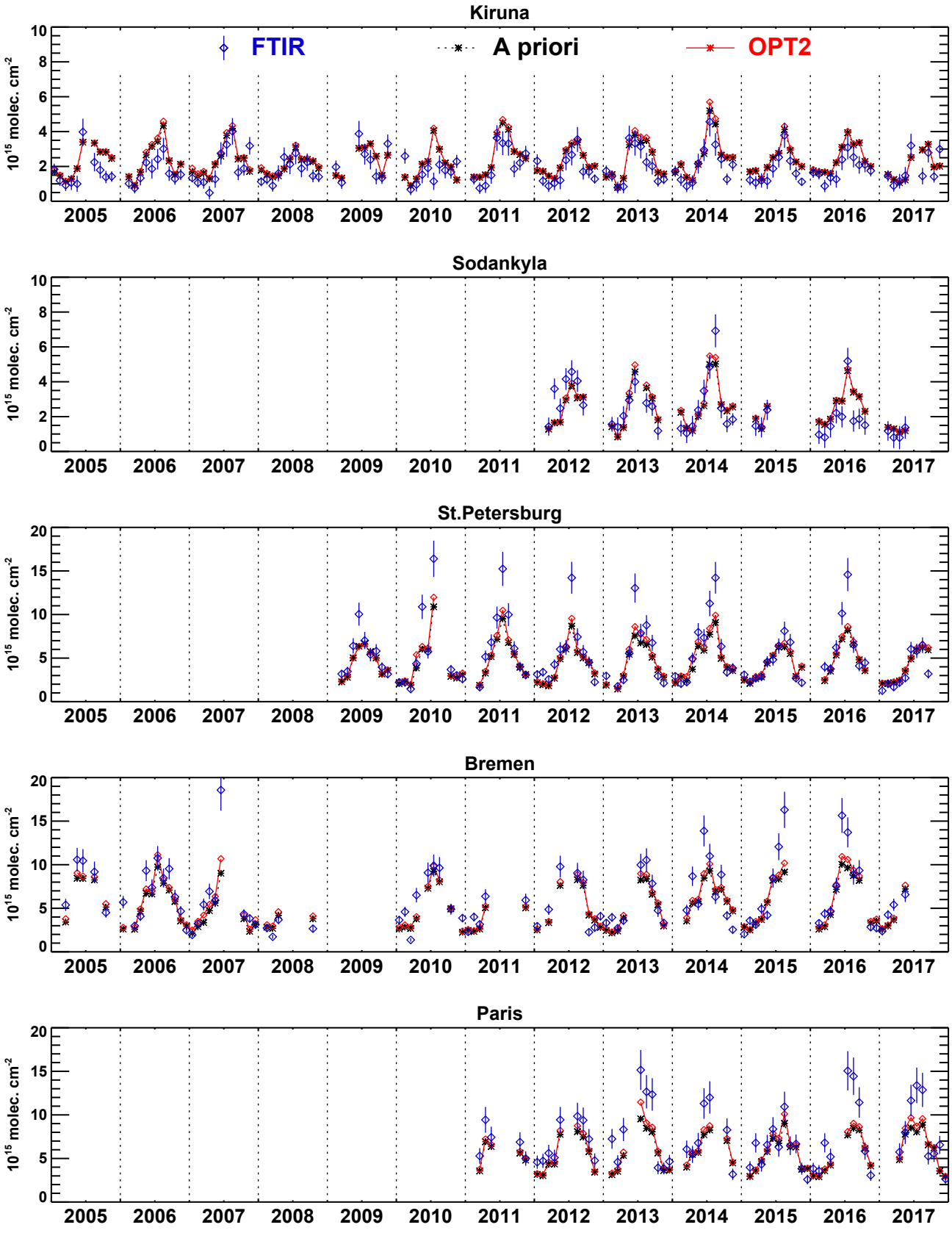

Figure S6. Observed (FTIR) and modelled monthly HCHO columns at Kiruna, Sodankylä, St. Petersburg, Bremen, and Paris. Symbols represent the mean FTIR columns and their systematic uncertainties. Black curve and asterisks: model with a priori emissions; red: OPT2 simulation constrained by bias-corrected OMI columns.

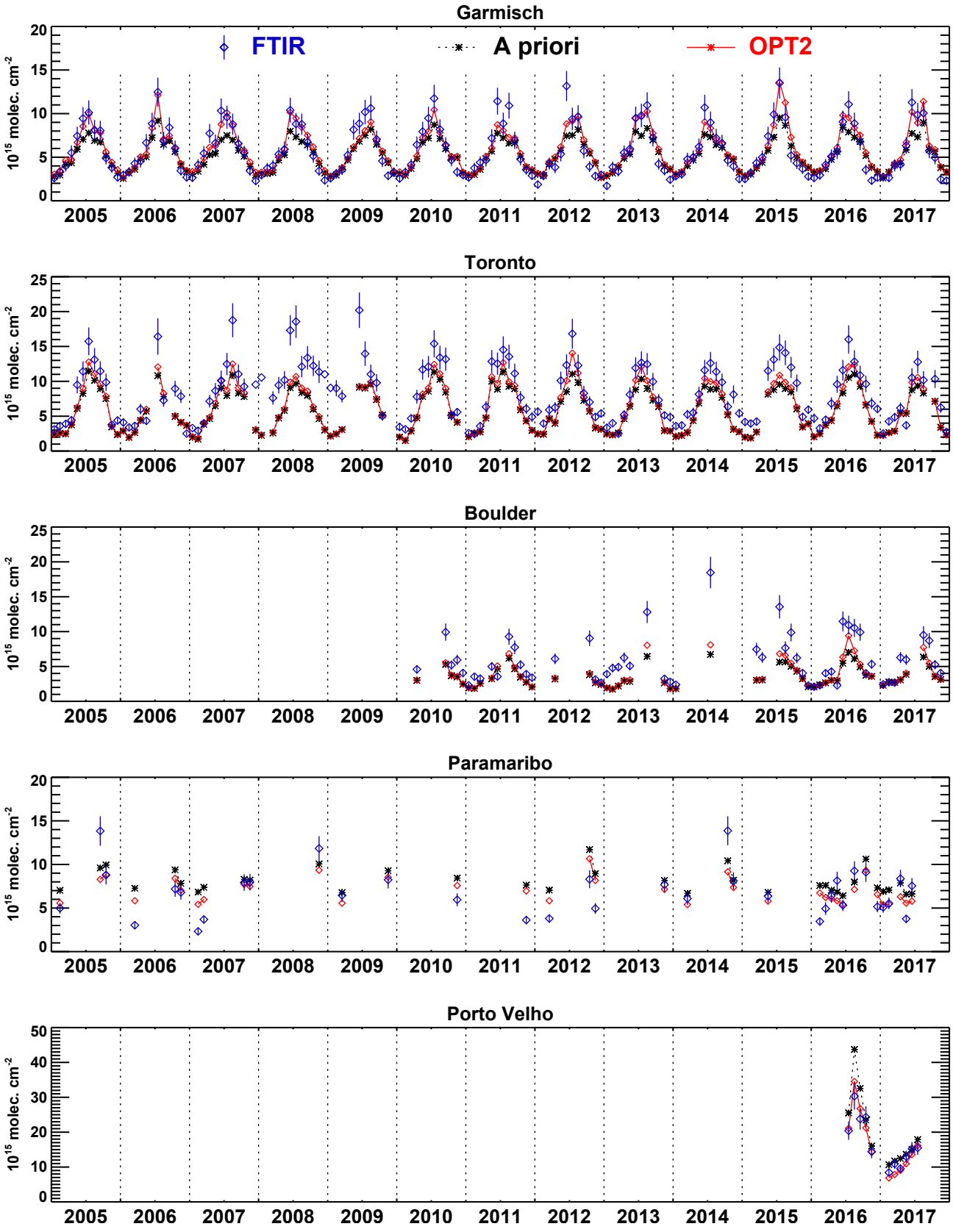

Figure S7. As previous figure, for Garmisch, Toronto, Boulder, Paramaribo, and Porto Velho.

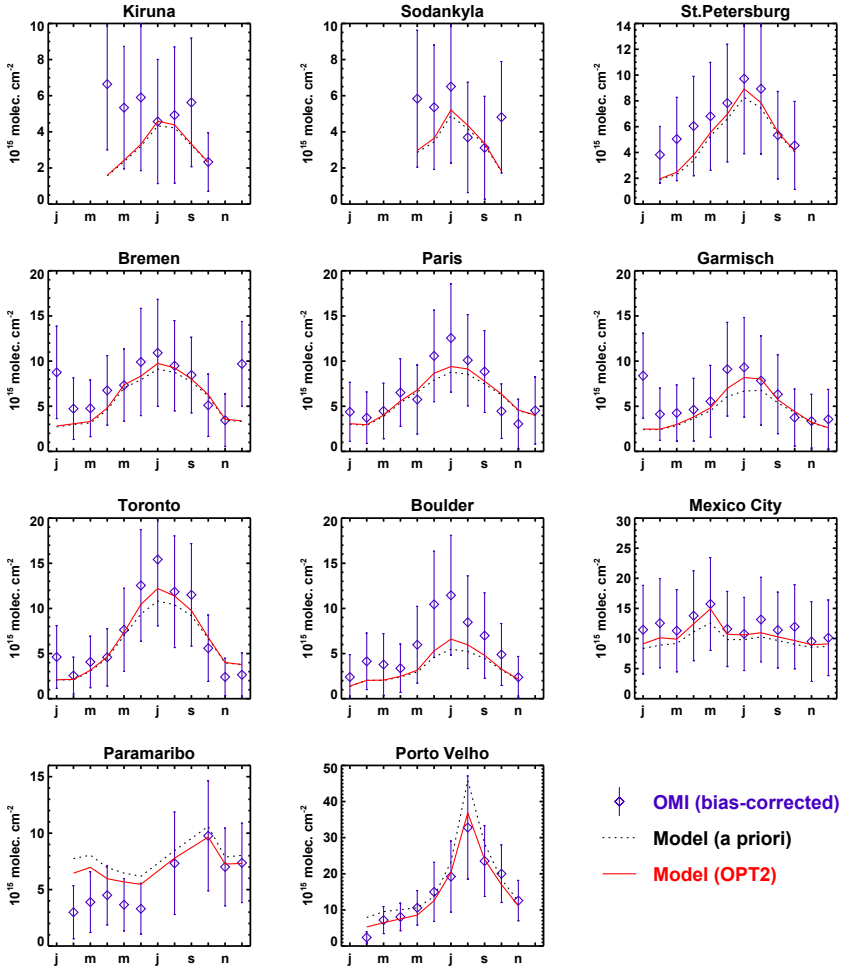

Figure S8. Average seasonal cycle of OMI and model HCHO columns at FTIR stations. Blue symbols with error bars represent the mean (bias-corrected) OMI columns and systematic uncertainties. Black dotted curve: model with a priori emissions; red: OPT2 simulation constrained by bias-corrected OMI columns.

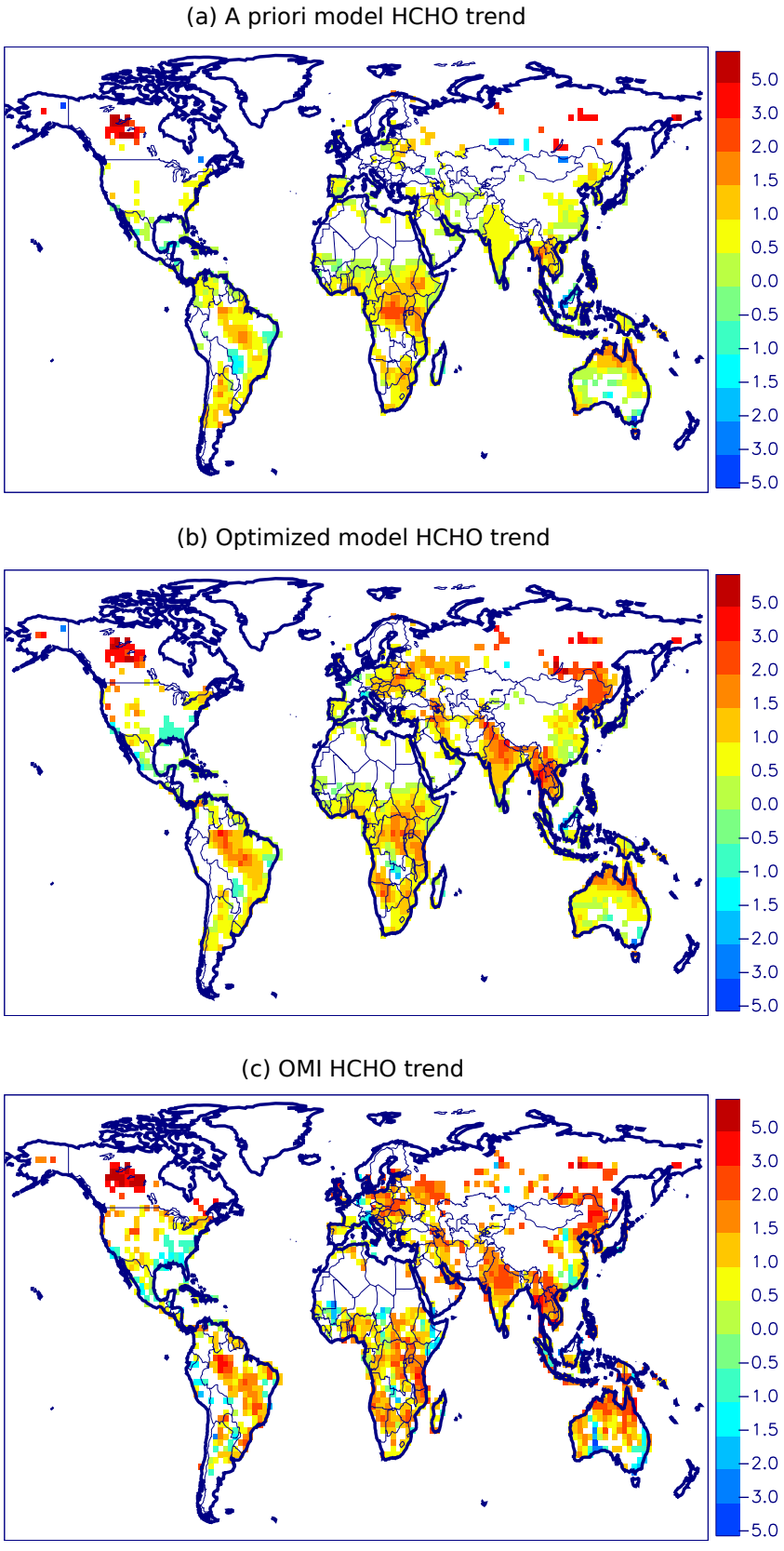

Figure S9. Trends (%/yr) over 2005–2016 of seasonally-averaged HCHO columns from (a) the a priori model simulation, (b) the optimized (OPT2) simulation, (c) the OMI retrieval. The HCHO columns are averaged over May–September in the Northern Hemisphere, January–May in the southern Tropics (0-30°S), and November–March in the Southern mid-latitudes ($> 30°$S).

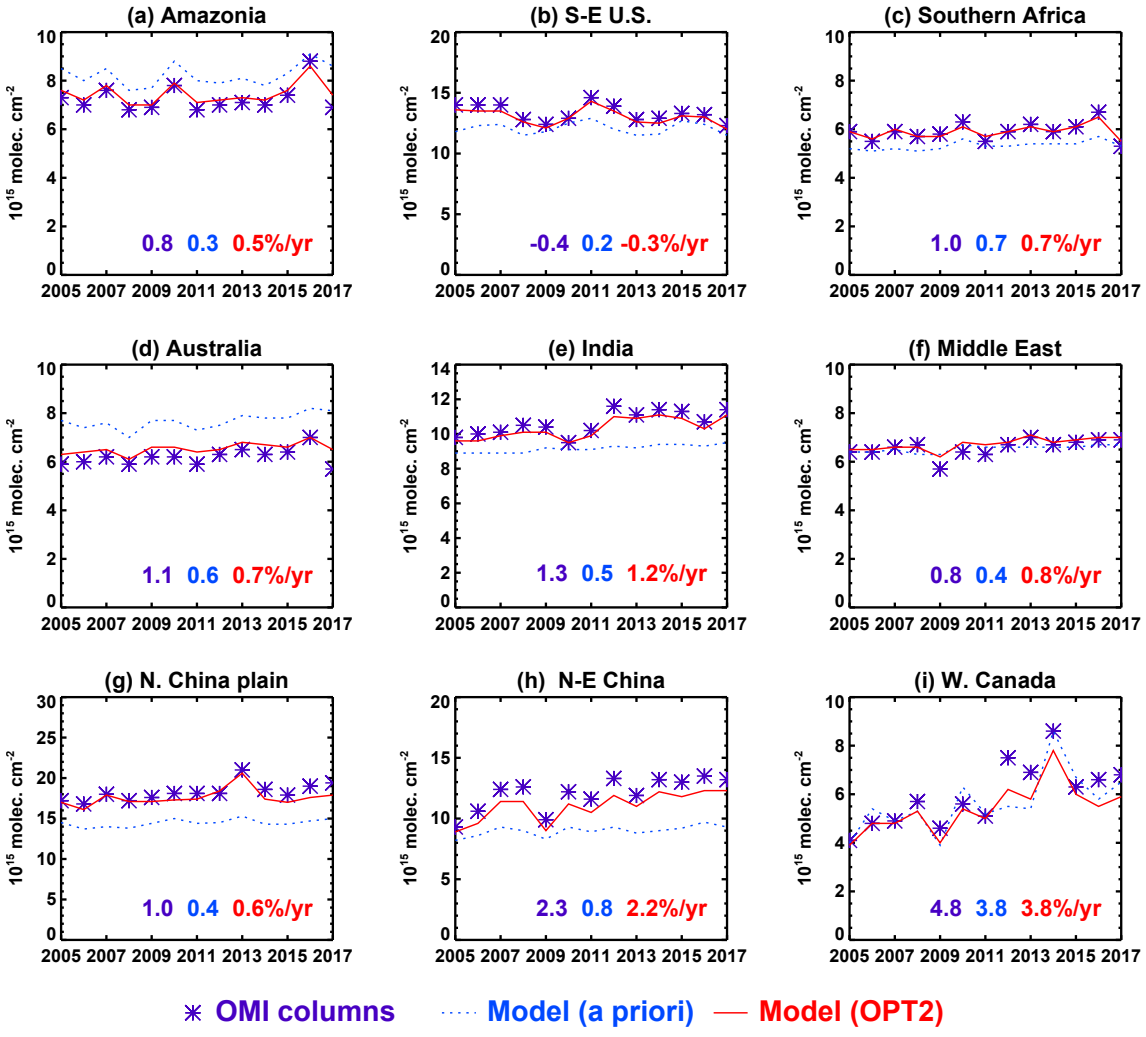

Figure S10. Seasonally-averaged (bias-corrected) HCHO columns averaged over the same large regions as in Fig. 13. Linear regression trends (2005–2016) are given inset. OMI: violet symbols; a priori model in blue, OPT2 model in red. The same averaging period is used as for Fig. S9.

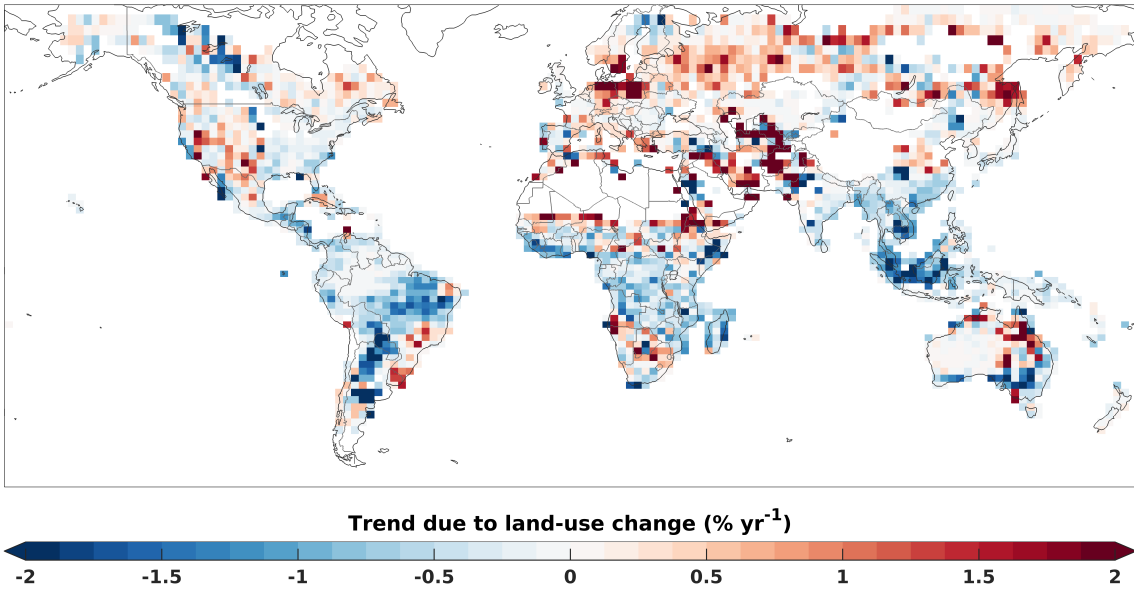

Figure S11. Trend in annual isoprene emissions due to land-use change calculated using MEGAN-MOHYCAN and tree cover distributions from the Global Forest Watch, following Opacka et al. (2021), for the 2005-2016 period at $2^\circ \times 2.5^\circ$ resolution. Pixels with mean isoprene emissions below 2.5×10^9 molec. $\mathrm{cm}^{-2}\, s^{-1}$ are left blank.